ChemComm

Intramolecular interaction suggests an autosuppression mechanism for the innate immune adaptor protein MyD88

Journal:	*ChemComm*
Manuscript ID	CC-COM-08-2018-006480.R2
Article Type:	Communication

Journal Name

COMMUNICATION

Intramolecular interaction suggests an autosuppression mechanism for the innate immune adaptor protein MyD88

Received 00th January 20xx,
Accepted 00th January 20xx

DOI: 10.1039/x0xx00000x

www.rsc.org/

Masatoshi Uno,[ab] Takahiro Watanabe-Nakayama,[c] Hiroki Konno,[c] Kenichi Akagi,[d] Naotaka Tsutsumi,[ab] Toshiyuki Fukao,[e] Masahiro Shirakawa,[b] Hidenori Ohnishi,*[e] Hidehito Tochio*[a]

MyD88 (myeloid differentiation factor 88) is an important protein in innate immunity. Two structural domains of MyD88 have been well characterized separately, but the global architecture of full-length MyD88 remained unclear. Here, we propose an autosuppressive mechanism of MyD88 regulated by the intramolecular interaction between the two domains.

MyD88 is an adaptor protein that functions in the innate immune response and inflammatory signaling,[1] which are activated by TLR (Toll-like receptor) and IL-1R (interleukin-1 receptor) family members. MyD88 comprises two protein-protein interaction modules: DD_{MyD88} (death domain) at the N-terminus and TIR_{MyD88} (Toll/IL-1R domain) at the C-terminus. These domains are connected by an ~35 amino acid residue linker (Fig. 1a).[2,3] The primary function of MyD88 has been well established: MyD88 bridges membrane receptors (TLRs and IL-1Rs) and cytosolic kinases called IRAKs (interleukin-1 receptor-associated kinases), in which the homo- and heterotypic interactions of both TIRs and DDs play critical roles. For instance, in TLR4 signaling, a component of pathogenic bacteria, lipopolysaccharide, binds the extracellular domain of TLR4 with cofactors, inducing homodimerization of the extracellular regions of TLR4 and bringing the cytosolic regions of two TLR4 molecules into close proximity,[4] enabling TIR_{TLR4} (TIR domain of TLR4) to dimerize underneath the membrane. The dimerized TIR_{TLR4} provides a combined surface that recruits Mal/TIRAP (MyD88 adapter-like/TIR-containing cytosolic adaptor proteins) and MyD88 via heteromeric oligomerization of the TIR domains of these proteins. Upon the formation of this complex containing the activated receptors, MyD88 starts to further recruit IRAK4 and IRAK1/2 to form a large protein complex termed the Myddosome, which is mediated by oligomeric interactions between the DDs of MyD88, IRAK4 and IRAK1/2. Myddosome formation results in the activation of IRAK4, which triggers downstream signaling to activate NF-κB and AP-1 to produce inflammatory cytokines.

The crystal structure of DD_{MyD88} in a complex with DD_{IRAK4} and DD_{IRAK2} was solved,[3] providing a clear picture of how DD_{MyD88}, DD_{IRAK4} and DD_{IRAK2} form the complex. However, although the structures of isolated TIRs of MyD88 and other TIR-containing adaptor proteins have been reported,[5–8] the details of how they form dimers/oligomers have not been well understood. Numerous biochemical studies of TIR_{MyD88} were conducted to identify sites on its surface that are critical for dimeric/oligomeric association, based on proposed structural models.[9] While DD_{MyD88} and TIR_{MyD88} have each been well characterized, their relative positions in a full-length context, namely, the global architecture of MyD88, have never been explored. In this study, to gain insights into the regulation mechanism of MyD88, which might be governed by its global architecture, we investigated the interdomain interaction of MyD88 by using NMR spectroscopy and HS-AFM (high speed atomic force microscopy).

We first recorded the NMR spectra of isolated ^{15}N-labeled TIR_{MyD88} in the absence or presence of DD_{MyD88} (Fig. 1b). The amide ^{1}H-^{15}N NMR signals of ^{15}N-TIR_{MyD88} in its free form were dispersedly distributed with substantial intensities, but many of these signals started to decrease when DD_{MyD88} was added (Fig. S1, ESI†). The reduction in NMR signals depended on the amount of added DD_{MyD88}, and the signals mostly disappeared when two eq (molecular equivalents) of DD_{MyD88} was added. Similar to other DD superfamily members,[10] DD_{MyD88} was previously demonstrated to form self-oligomers,[11,12] which underlie the signaling DD_{MyD88}-DD_{IRAK4}-DD_{IRAK2} complex, the Myddosome.[3] We thus interpreted the reduction in NMR signals as indicating that ^{15}N-TIR_{MyD88} bound such functionally relevant DD_{MyD88} oligomers but not resulting from non-specific aggregations (see Fig. S2). Once ^{15}N-TIR_{MyD88} binds to such oligomers, the NMR signals would broaden and weaken due to the shorter transverse relaxation time resulting from the

[a] Dept of Biophysics, Kyoto University, Kyoto, 606-8502, Japan. E-mail: tochio@mb.biophys.kyoto-u.ac.jp
[b] Dept of Molecular Engineering, Kyoto University, Kyoto, 615-8510, Japan.
[c] Kanazawa University, Nano Life Science Institute (WPI NanoLSI), Kanazawa, 920-1192, Japan.
[d] NIBIOHN, Section of Laboratory Equipment, Osaka, 567-0085, Japan
[e] Dept of Pediatrics, Gifu University, Gifu, 501-1194, Japan E-mail: ohnishih@gifu-u.ac.jp
†Electronic Supplementary Information (ESI) available: See DOI: 10.1039/x0xx00000x

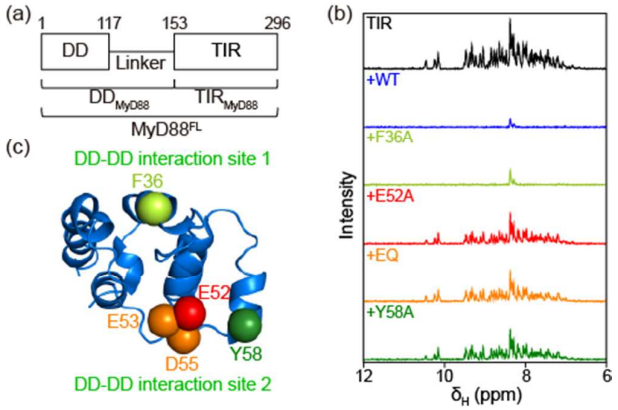

Fig. 1 NMR titration experiments to identify the binding sites of DD$_{MyD88}$ for ^{15}N-TIR$_{MyD88}$. (a) Schematic for the construction of MyD88. (b) ^{1}H 1D projections of the ^{1}H-^{15}N SOFAST-HMQC spectra of ^{15}N-TIR$_{MyD88}$ in the absence and presence of 2 eq of DD$_{MyD88}$ derivatives. (c) Position of the replaced amino acids (Cα) shown on the structure of DD$_{MyD88}$ (PDB ID: 3MOP).

slower molecular tumbling rate of the large molecular assembly.

After the direct interaction between DD$_{MyD88}$ and ^{15}N-TIR$_{MyD88}$ was revealed, we performed the same NMR titration experiment using DD$_{MyD88}$ derivatives harboring amino acid substitutions. Two single amino acid-substituted derivatives, DD$_{MyD88}$ (E52A) and DD$_{MyD88}$ (Y58A), and a triply substituted derivative (E52Q-E53Q-D55N) named DD$_{MyD88}$ (EQ) were tested (Fig. 1b). These derivatives did not show any decrease in the NMR signals of ^{15}N-TIR$_{MyD88}$ in the presence of DD$_{MyD88}$, indicating that the substituted residues (E52, E53, D55, and Y58) critically mediate the DD$_{MyD88}$-TIR$_{MyD88}$ interaction (Fig. 1c). A previous mutational study of MyD88 found that E52 and Y58 were important in recruiting IRAK4 (Fig. S3a).[13] Additionally, three anionic residues, E52, E53 and D55, were reported to play roles in mediating the interaction between DD$_{MyD88}$ and DD$_{IRAK4}$ (Fig. S3b).[3] Thus, it is possible that TIR$_{MyD88}$ interferes with the signaling-related DD$_{MyD88}$-DD$_{IRAK4}$ interaction by masking the interface on DD$_{MyD88}$, suggesting the possibility of an autosuppression mechanism of MyD88.

In contrast to these derivatives, DD$_{MyD88}$ (F36A) caused a decrease in the NMR signals, as wild-type DD$_{MyD88}$ (WT) did, demonstrating that F36 is not involved in the DD$_{MyD88}$-TIR$_{MyD88}$ interaction. In the crystal structure of the Myddosome assembly (complex of DD$_{MyD88}$-DD$_{IRAK4}$-DD$_{IRAK2}$), F36 is deeply involved in the DD$_{MyD88}$-DD$_{IRAK4}$ interface (Fig. S3a); thus, this residue is likely involved in the DD$_{MyD88}$-DD$_{IRAK4}$ interaction but not in the intramolecular DD$_{MyD88}$-TIR$_{MyD88}$ interaction.

Having demonstrated the interaction between TIR$_{MyD88}$ and DD$_{MyD88}$ and identified critical amino acid residues on DD$_{MyD88}$, we next explored the TIR$_{MyD88}$ surface for the sites responsible for binding DD$_{MyD88}$. To this end, a TCS-NMR (transfer cross-saturation NMR) experiment was conducted on the [^{2}H,^{15}N]-TIR$_{MyD88}$ sample.[14] In TCS-NMR, amino acid residues whose amide ^{1}H showed significantly decreased NMR signals were considered to have experienced saturation transfer at the molecular interface. As shown in Fig. 2a, the NMR signals of [^{2}H,^{15}N]-TIR$_{MyD88}$ displayed 20-30% or greater attenuation in

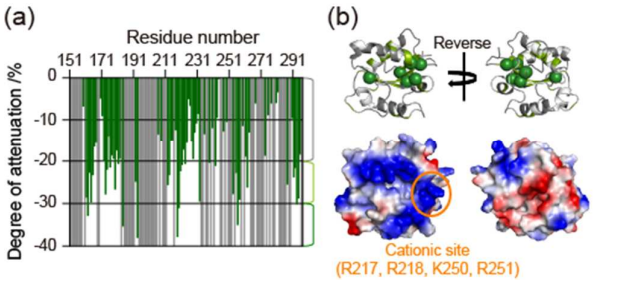

Fig. 2 TCS-NMR experiments to identify DD$_{MyD88}$ interaction sites on [^{2}H,^{15}N]-TIR$_{MyD88}$. (a) The degree of NMR signal attenuation of [^{2}H,^{15}N]-TIR$_{MyD88}$ caused by TCS plotted as a function of amino acid residue number. Gray columns indicate no data available. (b) The residues whose amide ^{1}H NMR signals substantially decreased are shown (Cα) in the ribbon model of TIR$_{MyD88}$ (PDB ID: 2Z5V), in which residues attenuated >30%, 20-30% and <20% and no data are illustrated as green spheres, yellow-green, white and gray, respectively. The surface electrostatic potential of the molecule is also shown. Blue and red indicate positive and negative potentials, respectively.

several regions, highlighting the residues that form contacts at the interface with DD$_{MyD88}$. These significantly attenuated residues (>30%), D162, V193, R218, M219, K256 and L293, illustrated as green spheres in Fig. 2b, were mostly found in the inside of the positively charged region, as mapped on the TIR structure in Fig. 2b, which comprises basic amino acid residues: R217, R218, K250 and R251. This finding is consistent with the negative charges of the interacting residues found in DD$_{MyD88}$. Therefore, electrostatic interactions likely dominate the TIR$_{MyD88}$-DD$_{MyD88}$ interface.

Although we have demonstrated the interactions between the separated TIR$_{MyD88}$ and DD$_{MyD88}$ by using NMR, in principle, those are intermolecular interactions. To experimentally verify the native intramolecular DD$_{MyD88}$-TIR$_{MyD88}$ interaction, analysis of MyD88^{FL} at the single molecule level is ideal. We thus employed HS-AFM, with which dynamic motions of single molecules can be visualized with nanometer spatial resolution and time resolution in the tens of milliseconds. Importantly, the technique can be applied to samples in aqueous media at room temperature and under ordinary pressure. Hence, the dynamics of global conformational changes under near-native conditions can be visualized, although the sample proteins must be weakly bound to the AFM stage. This association restricts the translational motion of the sample proteins to some extent. Nevertheless, HS-AFM would be sufficient to judge whether two domains are apart or in close proximity to make direct contact.

We first monitored MyD88^{FL} (WT) with HS-AFM on an APTES (3-aminopropyltriethoxysilane)-modified mica stage (Movie S1). Most of the MyD88^{FL} molecules were visualized as single particles (Fig. 3a). However, their surfaces are not smooth but have two humps, as clearly shown in Z-slice profiles, suggesting the existence of two subparticles tightly bound together to form a “closed” state (Fig. 3c, S4). We assumed the two humps to correspond to DD$_{MyD88}$ and TIR$_{MyD88}$, as the size of the particles was approximately consistent with the crystal structures. Notably, domain identification was impossible because of the similar sizes of the particles, with a size difference smaller than the spatial resolution of the measurement. In addition to the two-humped “closed”

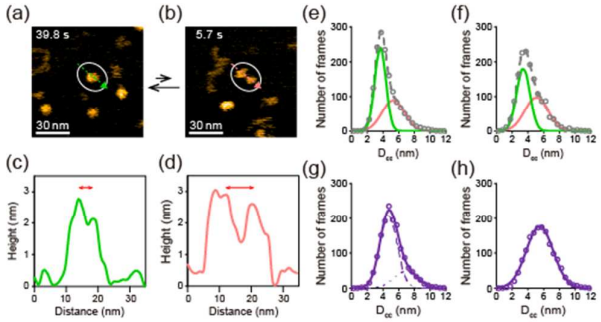

Fig. 3 Single-molecule analysis of MyD88^{FL} (WT) with HS-AFM. (a,b) Representative HS-AFM images of MyD88^{FL} in the closed state (a) and the open state (b) recorded on APTES-modified micas. These HS-AFM images were clipped from Movie S1. (Frame rate, 100 ms/frame; scan area, 100 × 100 nm^2 with 100 × 100 pixels; Z-scale, 4.3 nm; scale bars, 30 nm.) (c, d) Sectional views of the green and pink arrows in the AFM images in (a) and (b), respectively. (e,f) Histogram (open circles) for MyD88^{FL} (WT) recorded on an APTES-modified mica surface (e) and a mica surface (f). The gray dotted line represents the best fit to the data calculated by the summation of two Gaussian components corresponding to the closed state (green) and the open state (pink). (g) Histogram (open circles) for MyD88^{FL} (RA) recorded on an APTES-modified mica surface. The purple solid line represents the best fit with the summation of two Gaussian components (long broken line and short broken line). (h) Histogram (open circles) for MyD88^{FL} (EQ) recorded on the mica surface. The purple line represents the best single-Gaussian fit.

particles, we also found a subset of tandemly arranged pairs of particles, which changed their relative position from time to time. These particles may correspond to an elongated "open" state of MyD88^{FL}, in which no interdomain interaction occurs (Fig. 3b, d). Notably, the population of the open particles was smaller than that of the closed state.

D_{cc} (center-to-center distance between two subparticles or humps, the putative TIR and DD of MyD88^{FL}) was measured for each molecule in the AFM images and found to be distributed between 2 and 9 nm (Fig. 3e, gray).[15] The histogram of D_{cc} showed a skew shape and was explained by the summation of two Gaussian distributions with peaks at 3.66 ± 0.02 nm and 5.30 ± 0.04 nm (Fig. 3e, green and pink), which we think correspond to the D_{cc} distributions of the closed and open states, respectively.

Next, to determine whether the DD-TIR interaction in the closed state of MyD88^{FL} was indeed mediated by the key residues identified in our NMR experiments, we examined amino acid substitutions in MyD88^{FL}. We prepared a derivative harboring a substitution in the TIR domain, MyD88^{FL} (RA), in which R217 of TIR_{MyD88} of MyD88^{FL} was replaced with alanine. The AFM images recorded in this way showed a dramatic change in the distance distribution. Specifically, the D_{cc} distribution of MyD88^{FL} (RA) was dominated by a single Gaussian with a peak at 4.70 ± 0.03 nm, although a minor subset was found at 6.91 ± 0.04 nm and was even elongated (Fig. 3e vs. 3g). Importantly, the closed state of MyD88^{FL} (RA) was essentially absent (Fig. S5a, Table S1).

We then created MyD88^{FL} (EQ), in which E52, E53 and D55 in DD_{MyD88} were replaced by Gln or Asn (E52Q-E53Q-D55N), and conducted HS-AMF measurement of the sample. For this measurement, we employed an unmodified mica stage (see Fig. S6). As expected, the distance distribution of MyD88^{FL} (EQ) was best explained by a single Gaussian distribution with a peak at 5.49 ± 0.04 nm (Fig. 3f vs. 3h), indicating that the derivative existed mostly in the open state (Fig. S5b).

In this way, our AMF measurements demonstrated that MyD88^{FL} can adopt two distinct states (open and closed). In addition, the two variants, MyD88^{FL} (EQ) and MyD88^{FL} (RA), in which amino acid residues putatively mediating the DD_{MyD88}-TIR_{MyD88} interaction were mutated, were shown to rarely adopt the closed state. These findings suggest that the anionic sites of DD_{MyD88} and the cationic site of TIR_{MyD88} interact in an intramolecular fashion, most likely through the sites proposed in our NMR experiments.

In this study, we have demonstrated the intramolecular DD-TIR interaction of MyD88. In fact, another TIR-containing signaling adaptor protein, TRIF (TIR domain-containing adaptor molecule-inducing interferon-β), has been proposed to adopt an autosuppressed form, in which its N-terminal globular domain is presumed to bind TIR_{TRIF} in an intramolecular fashion that prevents the homodimerization of the TIR_{TRIF}, which is a necessary step for downstream signaling.[16–18] Such a scenario is also possible in MyD88 because the intramolecular DD_{MyD88}-TIR_{MyD88} interaction can suppress DD-DD oligomerization, as the sites on DD_{MyD88} for binding to TIR_{MyD88} identified in our study are also involved in the DD_{MyD88}-DD_{IRAK4} interaction in the Myddosome. Namely, the adoption of the closed state and the formation of the Myddosome seem to be mutually exclusive for MyD88. In other words, the closed state of MyD88 likely corresponds to its dormant form, whose activation is triggered only when the receptors dimerize and its interaction surface for TIR_{MyD88} forms a suitable shape.

Tumor genetic mutation analyses of liquid biopsies have identified gain-of-function mutations of MyD88, some of which are frequently found in lymphomas, such as the activated B-cell-like subtype of diffuse large B-cell lymphoma,[19] in which NF-κB and JAK kinase signaling were revealed to be constitutively activated, contributing to the proliferation and survival of malignant cells. One example of such a mutation is L265P (also annotated as L252P). Studies including molecular simulations[9,20,21] suggested that the mutation promotes the spontaneous oligomerization of TIR_{MyD88} (L265P), which can consequently cause the oligomerization of DDs and thus Myddosome formation. In this case, receptor activation is not necessary to trigger signaling, which is consistent with the constitutive activation observed in the reported lymphomas.[19,22,23] In agreement with this notion, we also found a strong tendency toward aggregate formation by isolated TIR_{MyD88} when the L265P mutation was introduced (Fig. S7). Thus, the intramolecular DD_{MyD88}-TIR_{MyD88} interaction observed in our study may be weaker than the TIR_{MyD88}-TIR_{MyD88} interaction once the L265P mutation is introduced. Hence, the closed state cannot be maintained, and the TIR_{MyD88} oligomers start to form the Myddosome. In addition, we propose an alternative mechanism: the L265P mutation may substantially weaken the DD_{MyD88}-TIR_{MyD88} interaction, making the dormant closed state much less populated and hence stimulating DD_{MyD88} oligomerization as well as TIR_{MyD88} oligomerization for Myddosome formation. This idea is well

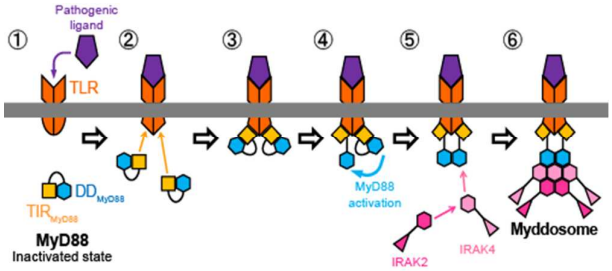

Fig. 4 The autosuppression model of MyD88. 1) Without ligand stimulation, MyD88 mostly exists in the closed state, in which both TIR_{MyD88} dimerization and DD_{MyD88} oligomerization with DD_{IRAKs} are strongly suppressed. 2-3) Once TIR_{TLR} forms an active dimer, MyD88 is recruited to and accumulated under the plasma membrane via the TIR-TIR interaction. As the local concentration of MyD88 increases, the molecules become open and initiate the formation of DD-DD oligomers via intermolecular interactions. 5-6) DD_{IRAKs} is recruited to yield the Myddosome complex. When the L265P mutation (or other analogous mutations) occurs in MyD88, TIR_{MyD88} gains a strong aggregation propensity, leading to the spontaneous formation of a dimer/oligomer. In addition, the closed state may be destabilized by the mutation. Both of these mutation outcomes promote Myddosome formation even without receptor dimerization, which would constitutively activate downstream signaling, as reported, contributing to tumor survival.

supported by the strong tendency of DD_{MyD88} to form active oligomers *in vitro* (Fig. S2) and in cells.[24]

Consistently, although endogenous $MyD88^{FL}$ is inactive as long as its upstream receptor is not activated, ectopic overexpression of $MyD88^{FL}$ was reported to constitutively activate its downstream signaling.[25] This result suggested that, at a physiological concentration of $MyD88^{FL}$, the intramolecular DD_{MyD88}-TIR_{MyD88} interaction is dominant,[26] resulting in a higher proportion of the closed state. However, at higher concentrations, the intermolecular interaction between DD_{MyD88} and DD_{MyD88} may become dominant. Moreover, our TCS-NMR experiments showed that R264 (R251) in TIR_{MyD88} resided at the binding interface for DD_{MyD88}. This residue is immediately next to L265 (L252), and hence, the L265P mutation can cause substantial changes in the shape of the DD_{MyD88}-TIR_{MyD88} interface. Intriguingly, another lymphoma-related mutation, M232T (M219T),[19] also occurs near this region (Fig. S8). These findings support the idea that the constant exposure of free DD_{MyD88} in the cytosol as a result of such mutations contributes at least partially to the constitutive activation of MyD88-dependent signaling.

In this study, we demonstrated the DD-TIR intramolecular interaction of MyD88 by using NMR spectroscopy and HS-AFM. Real-time monitoring by AFM revealed that $MyD88^{FL}$ can adopt the closed form, in which DD_{MyD88} and TIR_{MyD88} are tightly bound together, which allowed us to propose the autosuppression mechanism for the molecule (Fig. 4). Tight regulation implemented by such a mechanism would be critical because the unregulated activation of MyD88-dependent signaling can lead to innate immune and inflammatory disorders that severely damage organisms.

Conflicts of interest

There are no conflicts to declare.

Notes and references

1 J. Deguine and G. M. Barton, *F1000Prime Rep.*, 2014, **6**, 1–7.
2 M. Avbelj, S. Horvat and R. Jerala, *J. Immunol.*, 2011, **187**, 2394–2404.
3 S. C. Lin, Y. C. Lo and H. Wu, *Nature*, 2010, **465**, 885–890.
4 S. Latty, J. Sakai, L. Hopkins, B. Verstak, T. Paramo, N. A. Berglund, N. J. Gay, P. J. Bond, D. Klenerman and C. E. Bryant, *Elife*, 2018, **7**, 1–16.
5 H. Ohnishi, H. Tochio, Z. Kato, K. E. Orii, A. Li, T. Kimura, H. Hiroaki, N. Kondo and M. Shirakawa, *Proc. Natl. Acad. Sci. U. S. A.*, 2009, **106**, 10260–10265.
6 Z. Lin, J. Lu, W. Zhou and Y. Shen, *PLoS One*, 2012, **7**, e34202.
7 Y. Enokizono, H. Kumeta, K. Funami, M. Horiuchi, J. Sarmiento, K. Yamashita, D. M. Standley, M. Matsumoto, T. Seya and F. Inagaki, *Proc. Natl. Acad. Sci. U. S. A.*, 2013, **110**, 1–6.
8 S. Halabi, E. Sekine, B. Verstak, N. J. Gay and M. C. Moncrieffe, *J. Biol. Chem.*, 2017, **292**, 652–660.
9 L. Vyncke, C. Bovijn, E. Pauwels, T. Van Acker, E. Ruyssinck, E. Burg, J. Tavernier and F. Peelman, *Structure*, 2016, **24**, 437–447.
10 P. R. Vajjhala, T. Ve, A. Bentham, K. J. Stacey and B. Kobe, *Mol. Immunol.*, 2017, **86**, 23–37.
11 P. G. Motshwene, M. C. Moncrieffe, J. G. Grossmann, C. Kao, M. Ayaluru, A. M. Sandercock, C. V. Robinson, E. Latz and N. J. Gay, *J. Biol. Chem.*, 2009, **284**, 25404–25411.
12 T. Yamamoto, N. Tsutsumi, H. Tochio, H. Ohnishi, K. Kubota, Z. Kato, M. Shirakawa and N. Kondo, *Mol. Immunol.*, 2014, **58**, 66–76.
13 M. Loiarro, G. Gallo, N. Fantò, R. De Santis, P. Carminati, V. Ruggiero and C. Sette, *J. Biol. Chem.*, 2009, **284**, 28093–28103.
14 I. Shimada, *Methods Enzymol.*, 2005, **394**, 483–506.
15 N. Kodera, K. Uchida, T. Ando and S. I. Aizawa, *J. Mol. Biol.*, 2015, **427**, 406–414.
16 M. Tatematsu, A. Ishii, H. Oshiumi, M. Horiuchi, F. Inagaki, T. Seya and M. Matsumoto, *J. Biol. Chem.*, 2010, **285**, 20128–20136.
17 M. O. Ullah, T. Ve, M. Mangan, M. Alaidarous, M. J. Sweet, A. Mansell and B. Kobe, *Acta Crystallogr. Sect. D Biol. Crystallogr.*, 2013, **69**, 2420–2430.
18 J. Mahita and R. Sowdhamini, *Biol. Direct*, 2017, **12**, 1–15.
19 V. N. Ngo, R. M. Young, R. Schmitz, S. Jhavar, W. Xiao, K. H. Lim, H. Kohlhammer, W. Xu, Y. Yang, H. Zhao, A. L. Shaffer, P. Romesser, G. Wright, J. Powell, A. Rosenwald, H. K. Muller-Hermelink, G. Ott, R. D. Gascoyne, J. M. Connors, L. M. Rimsza, E. Campo, E. S. Jaffe, J. Delabie, E. B. Smeland, R. I. Fisher, R. M. Braziel, R. R. Tubbs, J. R. Cook, D. D. Weisenburger, W. C. Chan and L. M. Staudt, *Nature*, 2011, **470**, 115–121.
20 M. Avbelj, O.-O. Wolz, O. Fekonja, M. Ben ina, M. Repi, J. Mavri, J. Kruger, C. Scharfe, M. Delmiro Garcia, G. Panter, O. Kohlbacher, A. N. R. Weber and R. Jerala, *Blood*, 2014, **124**, 3896–3904.
21 C. Zhan, R. Qi, G. Wei, E. Guven-Maiorov, R. Nussinov and B. Ma, *Protein Eng. Des. Sel.*, 2016, **29**, 347–354.
22 S. P. Treon, L. Xu, G. Yang, Y. Zhou, X. Liu, Y. Cao, P. Sheehy, R. J. Manning, C. J. Patterson, C. Tripsas, L. Arcaini, G. S. Pinkus, S. J. Rodig, A. R. Sohani, N. L. Harris, J. M. Laramie, D. A. Skifter, S. E. Lincoln and Z. R. Hunter, *N. Engl. J. Med.*, 2012, **367**, 826–833.
23 X. Yu, W. Li, Q. Deng, L. Li, E. D. Hsi, K. H. Young, M. Zhang and Y. Li, *Cancer Res.*, 2018, **78**, 2457–2462.
24 T. Nishiya, E. Kajita, T. Horinouchi, A. Nishimoto and S. Miwa, *FEBS Lett.*, 2007, **581**, 3223–3229.
25 R. Medzhitov, P. Preston-hurlburt, E. Kopp, A. Stadlen, C. Chen, S. Ghosh and C. A. Janeway, *Mol. Cell*, 1998, **2**, 253–258.
26 V. M. Krishnamurthy, V. Semetey, P. J. Bracher, N. Shen and G. M. Whitesides, *J. Am. Chem. Soc.*, 2007, **129**, 1312–1320.